



HAL
open science

High temperature thermoelectric properties of the type-I clathrate $\text{Ba}_8\text{AuxSi}_{46-x}$

Christophe Candolfi, Umut Aydemir, Michael Baitinger, Niels Oeschler,
Franck Steglich, Yuri Grin

► **To cite this version:**

Christophe Candolfi, Umut Aydemir, Michael Baitinger, Niels Oeschler, Franck Steglich, et al.. High temperature thermoelectric properties of the type-I clathrate $\text{Ba}_8\text{AuxSi}_{46-x}$. *Journal of Applied Physics*, 2012, 111 (4), pp.043706. 10.1063/1.3682585 . hal-03997305

HAL Id: hal-03997305

<https://hal.science/hal-03997305>

Submitted on 20 Feb 2023

HAL is a multi-disciplinary open access archive for the deposit and dissemination of scientific research documents, whether they are published or not. The documents may come from teaching and research institutions in France or abroad, or from public or private research centers.

L'archive ouverte pluridisciplinaire **HAL**, est destinée au dépôt et à la diffusion de documents scientifiques de niveau recherche, publiés ou non, émanant des établissements d'enseignement et de recherche français ou étrangers, des laboratoires publics ou privés.



High temperature thermoelectric properties of the type-I clathrate $\text{Ba}_8\text{AuxSi}_{46-x}$

C. Candolfi, U. Aydemir, M. Baitinger, N. Oeschler, F. Steglich et al.

Citation: *J. Appl. Phys.* **111**, 043706 (2012); doi: 10.1063/1.3682585

View online: <http://dx.doi.org/10.1063/1.3682585>

View Table of Contents: <http://jap.aip.org/resource/1/JAPIAU/v111/i4>

Published by the [American Institute of Physics](http://www.aip.org).

Related Articles

Thermoelectric properties of Zn-doped GaSb

J. Appl. Phys. **111**, 043704 (2012)

Enhancement of thermoelectric properties in graphene nanoribbons modulated with stub structures

Appl. Phys. Lett. **100**, 073105 (2012)

The effect of crystallite size on thermoelectric properties of bulk nanostructured magnesium silicide (Mg_2Si) compounds

Appl. Phys. Lett. **100**, 073107 (2012)

Interplay of point defects, biaxial strain, and thermal conductivity in homoepitaxial SrTiO_3 thin films

Appl. Phys. Lett. **100**, 061904 (2012)

First principles study of Seebeck coefficients of doped semiconductors $\text{ZnTe}_{1-x}\text{Fx}$ and $\text{ZnTe}_{1-y}\text{Ny}$

J. Appl. Phys. **111**, 033701 (2012)

Additional information on *J. Appl. Phys.*

Journal Homepage: <http://jap.aip.org/>

Journal Information: http://jap.aip.org/about/about_the_journal

Top downloads: http://jap.aip.org/features/most_downloaded

Information for Authors: <http://jap.aip.org/authors>

ADVERTISEMENT

	Working @ low temperatures? Contact Janis for Cryogenic Research Equipment Click here to browse our site at www.janis.com	
---	---	---

High temperature thermoelectric properties of the type-I clathrate $\text{Ba}_8\text{Au}_x\text{Si}_{46-x}$

C. Candolfi,^{a),b)} U. Aydemir, M. Baitinger, N. Oeschler, F. Steglich, and Yu. Grin^{a)}

Max-Planck-Institut für Chemische Physik fester Stoffe, Nöthnitzer Str. 40, 01187 Dresden, Germany

(Received 7 October 2011; accepted 7 December 2011; published online 22 February 2012)

The thermoelectric properties of the type-I clathrate $\text{Ba}_8\text{Au}_x\text{Si}_{46-x}$ ($4.10 \leq x \leq 6.10$) were characterized from 300 to 700 K. Increasing the Au concentration leads to a transition from an *n*-type ($x < 5.43$) to a *p*-type ($x \geq 5.43$) electrical conduction. The experimental data are well described by a single-parabolic-band model assuming a single scattering mechanism of the charge carriers in this temperature range. The lattice thermal conductivity, inferred from degeneracy-adjusted Lorenz numbers, is low regardless of the composition. However, the measured values are significantly lower in the *p*-type samples possibly due to a combination of a higher degree of disorder in the crystal structure at high Au contents and an enhanced phonon-charge carrier coupling. Even though high thermopower values are achieved, the high electrical resistivity remains the main obstacle to push the dimensionless figure of merit ZT (~ 0.2 at around 600 K for $x = 5.59$) beyond the level of the best Si-based clathrate compounds. © 2012 American Institute of Physics. [doi:10.1063/1.3682585]

I. INTRODUCTION

The last decades have witnessed an increasing attention in type-I clathrate compounds due to their interesting and unusual transport properties.^{1–3} One of the prominent features of these materials lies in their crystal structures composed of polyhedral cages, formed by covalently bonded host framework, in which guest atoms can be entrapped (Figure 1).^{1–3} The influence of the crystal structure on the electronic and thermal transport was therefore at the aim of an ever-growing number of studies. In particular, the ability of some of these materials to mimic the thermal transport of glassy systems places naturally clathrates as potential candidates for thermoelectric applications.^{4–9} The low thermal conductivity inherent to this class of compounds is one of the requirements which need to be achieved in thermoelectric materials.^{1,10} This can be straightforwardly understood by considering the dimensionless figure of merit $ZT = \alpha^2 T / \rho \kappa = PT / \kappa$ which represents the basic criterion to determine the thermoelectric potential of a material.¹⁰ In this formula, α is the Seebeck coefficient or thermopower, ρ is the electrical resistivity, κ is the thermal conductivity, T is the absolute temperature, and $P = \alpha^2 / \rho$ is the power factor. To reach high ZT values, an ideal thermoelectric material with large thermopower should therefore conduct heat as poorly as glass, but maintaining good electrical transport properties associated with crystalline solids.¹⁰

While a large number of studies dealing with the thermoelectric properties of Ge-based type-I clathrates were reported in the last few years, the investigations devoted to the Si-based analogues remain so far rather scarce.¹ Interest-

ing results were nevertheless reported in $\text{Ba}_8\text{Ga}_x\text{Si}_{46-x}$ with maximum ZT of ~ 0.75 and 0.87 at 1000 and 850 K, respectively. For $x \sim 16$, these values are similar to ZT obtained in polycrystalline $\text{Ba}_8\text{Ga}_{16}\text{Ge}_{30}$ (~ 0.8 at 950 K) showing that the Si-based clathrates may also constitute a class of efficient thermoelectric materials.^{11–14} The good thermoelectric properties of the $\text{Ba}_8\text{Ga}_{16}\text{Si}_{30}$ compound originate from the possibility to drive the system into a semiconducting state expected to develop at $x = 16$, when the charge balance is achieved following the Zintl-Klemm concept, i.e., $(\text{Ba}^{2+})_8(\text{Ga}^-)_{16}(\text{Si}^0)_{30}$.^{11,12,15,16} Slight variations of the Ga content around this value lead to highly doped semiconductors allowing a fine tuning of the power factor. Several other elements, namely Al, Au, and Ag, are known to open a gap near the Fermi level, potentially enabling to reach similar or even higher ZT values.^{17–20} It is, therefore, of prime importance to further investigate the influence of these elements to determine whether or not a significant improvement of the thermoelectric properties can be achieved.

In this regard, we recently performed a thorough experimental and theoretical study of the low-temperature transport properties of the phase $\text{Ba}_8\text{Au}_x\text{Si}_{46-x}$ for $4.10 \leq x \leq 6.10$.²¹ In agreement with simple electron counting rules and prior investigations by Jaussaud *et al.*,²³ a transition from *n*-type to *p*-type conduction was confirmed to set in near $x \sim 5.33$. Since clathrate compounds may be intriguing candidates for thermoelectric applications at high temperatures, it is essential to extend these measurements to above room temperature to properly assess the thermoelectric potential of this phase.

Here, we provide a detailed study of the thermoelectric properties of the $\text{Ba}_8\text{Au}_x\text{Si}_{46-x}$ system from 300 up to 700 K. Our results show that substituting Si by Au helps to reduce the thermal conductivity. The impact of Au substitution on the thermal transport is more pronounced in the *p*-type compounds and might be related to an enhanced phonon-charge carrier coupling and to the mixed occupation of Au on two

^{a)} Authors to whom correspondence should be addressed. Electronic addresses: christophe.candolfi@ijl.nancy-universite.fr and grin@cpfs.mpg.de.

^{b)} Present address: Institut Jean Lamour, UMR 7198 CNRS-Nancy Université-UPVM, Ecole Nationale Supérieure des Mines de Nancy, Parc de Saurupt, F-54042 Nancy, France.

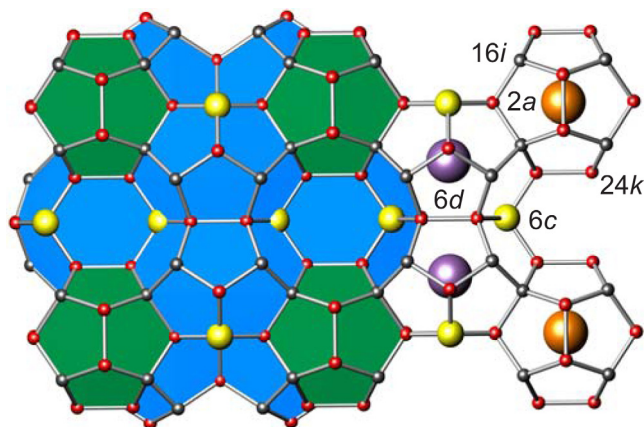


FIG. 1. (Color online) Crystal structure of the type-I clathrate. The framework atoms are located at the $6c$, $16i$, and $24k$ sites, while the “guest” atoms are located at the $2a$ and $6d$ sites. The clathrate framework is built upon two types of polyhedra: the pentagonal dodecahedra (centered by the $2a$ site) and the tetrakaidecahedra (centered by the $6d$ site).

distinct Si sites of the crystal structure.²² The data are further analyzed within a single parabolic band model which gives a pertinent theoretical background for understanding the transport in these compounds.

II. EXPERIMENTAL DETAILS

Polycrystalline $\text{Ba}_8\text{Au}_x\text{Si}_{46-x}$ samples with nominal compositions $x=4.0, 4.75, 5.15, 5.30, 5.45, 5.60,$ and 6.0 were prepared from crystalline Ba pieces (ChemPur, 99.9%), Au powders (ChemPur, 99.9%), and Si pieces (ChemPur, 99.9999%). In the first step, stoichiometric amounts of the elements were placed in glassy carbon crucibles and melted using an induction furnace under inert atmosphere. Subsequently, the molten ingots were quenched between two steel plates. For annealing, the ingots were transferred into glassy carbon crucibles, sealed in tantalum tubes and jacketed in quartz ampoules. After three weeks tempering at 900°C , the ampoules were quenched in water. The clathrate phase was observed to be stable on air as well as against dilute acids and bases. Throughout this paper, the labelling of the samples refers to the actual compositions.

Structural and chemical characterizations were carried out through powder x-ray diffraction (PXRD), energy dispersive x-ray spectroscopy (EDXS), and wavelength dispersive x-ray spectroscopy (WDXS). PXRD and WDXS analyses have shown that all samples are homogeneous with a good correlation between the nominal and actual compositions (Table I). Small amounts of α -Si, which never exceeds 3–4 wt.%, were detected in each sample (Figure 2).²¹ Single crystal x-ray diffraction analysis showed that the clathrate phase crystallizes in the space group $Pm\bar{3}n$.^{22,23} In the first report by Cordier and Woll,²² Au atoms were refined only at the $6c$ site which is the position preferentially occupied by most of the transition metals in substituted clathrates.^{1,24,25} However, in the more recent investigation performed by Jaussaud *et al.*²³ on clathrates with the compositions $\text{Ba}_8\text{Au}_{5.43}\text{Si}_{40.57}$ and $\text{Ba}_8\text{Au}_{5.89}\text{Si}_{40.11}$, small amounts of Au atoms were also refined at the $24k$ site.²³ Here, XRD investi-

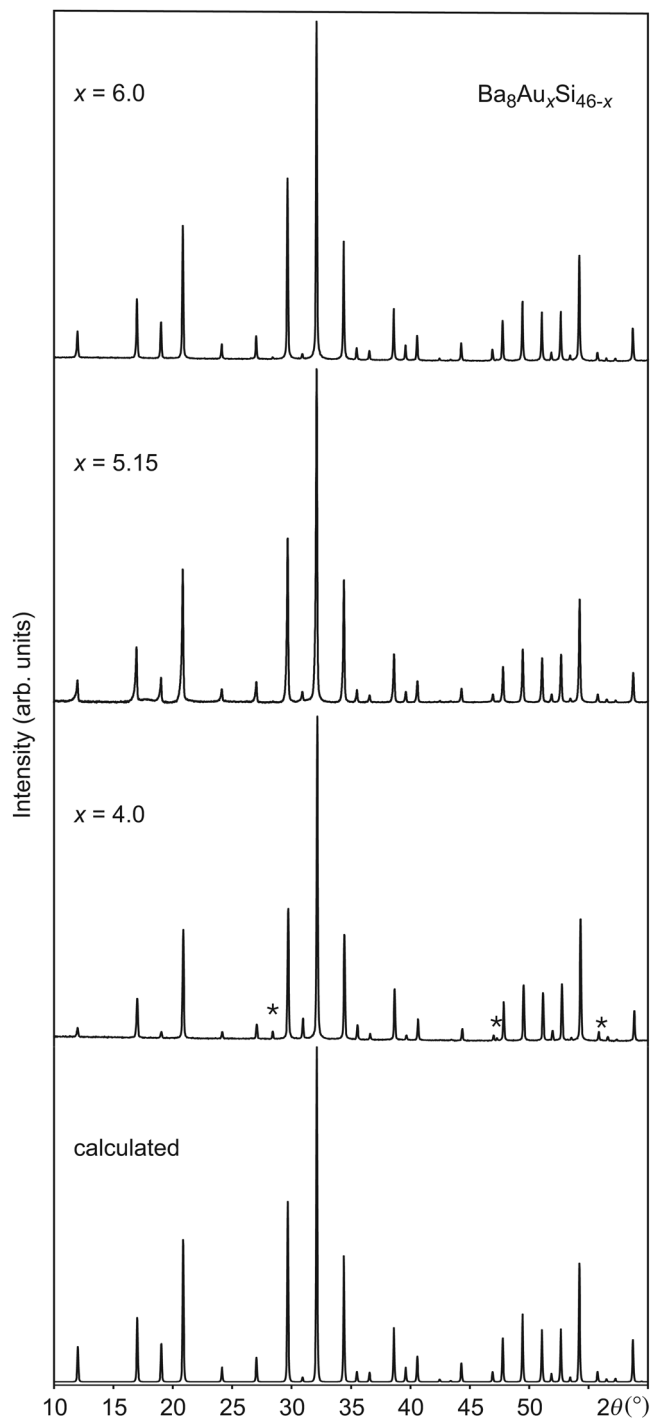


FIG. 2. PXRD patterns ($\text{Cu-K}\alpha_1$ radiation) of $\text{Ba}_8\text{Au}_x\text{Si}_{46-x}$ samples with nominal compositions $x=4.0, 5.15,$ and 6.0 together with the calculated profile based on a single crystal analysis for $x=5.89$.²³ The asterisks mark the position of the three most intense α -Si reflections.

gations were performed on a single crystal selected from $\text{Ba}_8\text{Au}_6\text{Si}_{40}$ sample. Our study confirms the results obtained by Jaussaud *et al.*²³ i.e., Au atoms mainly occupy the $6c$ site, a small amount being located on the $24k$ site (~ 0.5 Au atoms). From this analysis, a final conclusion about the presence of vacancies could not be drawn (if any, their concentration should be small, less than ~ 0.3 per formula unit). The lattice parameters a of the clathrate phase were refined from PXRD data with the WinCSD program package using

TABLE I. Nominal, measured compositions (WDXS) and lattice parameters (a) of $\text{Ba}_8\text{Au}_x\text{Si}_{46-x}$.

Nominal composition	WDXS composition	a (Å)
$\text{Ba}_8\text{Au}_4\text{Si}_{42}$	$\text{Ba}_{8.00(3)}\text{Au}_{4.10(5)}\text{Si}_{40.84(5)}$	10.39768(8)
$\text{Ba}_8\text{Au}_{4.75}\text{Si}_{41.25}$	$\text{Ba}_{8.00(2)}\text{Au}_{4.85(2)}\text{Si}_{39.72(4)}$	10.4084(1)
$\text{Ba}_8\text{Au}_{5.15}\text{Si}_{40.85}$	$\text{Ba}_{8.00(2)}\text{Au}_{5.14(2)}\text{Si}_{39.51(2)}$	10.41473(8)
$\text{Ba}_8\text{Au}_{5.30}\text{Si}_{40.70}$	$\text{Ba}_{8.00(3)}\text{Au}_{5.43(5)}\text{Si}_{39.76(6)}$	10.41615(9)
$\text{Ba}_8\text{Au}_{5.45}\text{Si}_{40.55}$	$\text{Ba}_{8.00(2)}\text{Au}_{5.59(2)}\text{Si}_{39.01(3)}$	10.41747(8)
$\text{Ba}_8\text{Au}_{5.60}\text{Si}_{40.40}$	$\text{Ba}_{8.00(3)}\text{Au}_{5.76(2)}\text{Si}_{39.21(4)}$	10.41761(9)
$\text{Ba}_8\text{Au}_6\text{Si}_{40}$	$\text{Ba}_{8.00(2)}\text{Au}_{6.10(2)}\text{Si}_{38.97(4)}$	10.41767(9)

LaB_6 as internal standard (Table I).²⁶ The increase in the lattice parameter up to $x = 5.59$ is consistent with an increase in the Au concentration. Interestingly, a remains almost constant thereafter which might be caused by the presence of some Au atoms on other crystallographic sites and/or of the presence of vacancies.

Thermopower and electrical resistivity were simultaneously measured over the 300–700 K temperature range with a commercial setup (ZEM-3, UlvacRiko) on bar-shaped specimens, cut with a diamond-wire saw from the annealed ingots into typical dimensions of $2 \times 2 \times 6 \text{ mm}^3$. It is worth mentioning that all the samples used in the present study are those used for the transport property measurements at low temperatures.²¹ Prism-shaped specimens ($6 \times 6 \times 1 \text{ mm}^3$) were used to measure, in the same temperature range, the thermal diffusivity a which is related to the thermal conductivity κ via $\kappa = aC_p\rho_V$, where C_p is the specific heat and ρ_V is the density. The thermal diffusivity and specific heat were measured by a laser flash technique (LFA 427, Netzsch) and by a differential scanning calorimetry technique (Pegasus, Netzsch), respectively. To evaluate $\rho_V(T)$, the value of the thermal-expansion coefficient, α_T , measured on a $\text{Ba}_8\text{Au}_5\text{Si}_{41}$ sample by Falmbigl *et al.*²⁷ was used ($\alpha_T \sim 7.3 \times 10^{-6} \text{ K}^{-1}$ at 300 K). As a first approximation, the value of α_T was considered to be temperature- and composition-independent. An overall good agreement between the low-temperature and high-temperature measurements was observed, the deviation at 300 K being at most 12%.

III. RESULTS AND DISCUSSION

A. Electronic properties

Figure 3 depicts the temperature dependence of the thermopower. In agreement with the low-temperature data, the

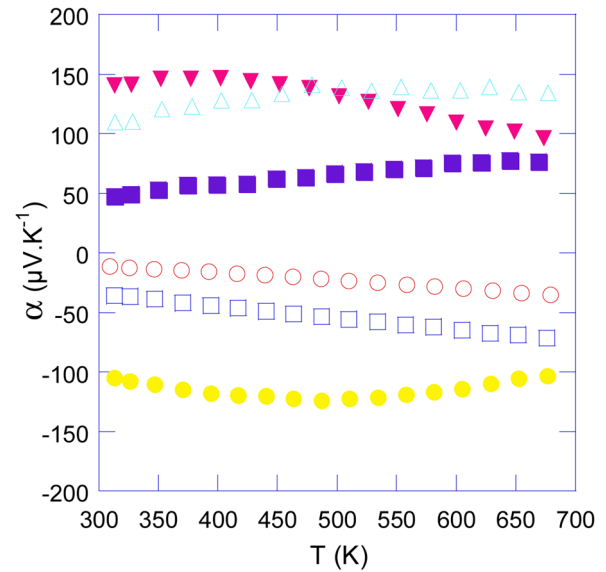


FIG. 3. (Color online) Thermopower, α , as a function of the temperature of the $x=4.10$ (○), 4.85 (□), 5.14 (●), 5.43 (▼), 5.59 (△), and 6.10 (■) samples.

n -type electrical conduction prevailing for $x < 5.43$ and characterized by negative α values turns into a p -type conduction above this concentration.²¹ The magnitude of $|\alpha|$ increases with the Au content, both in the n -type and p -type regions, reflecting the variation in the carrier concentration with x (Table II). At 300 K, the α values are significantly higher than those measured in the Al- or Ga-substituted Si-based clathrates.^{11,12,18,20} As we shall see below, this difference is mainly due to larger effective mass of the charge carriers in the present system. Further, the overall behaviour of $\alpha(T)$ against the Au content is consistent with the picture revealed at low temperatures: here, the metallic behaviour characterizing the $x=4.10$ sample smoothly evolves into a highly doped semiconducting behaviour on approaching $x=5.33$, then turns into a semiconducting behaviour ($x=5.43$) before switching back to a metallic-like behaviour at higher Au contents.

The decrease in $|\alpha|$ observed in the $x=5.14$, 5.43, and 5.59 samples with increasing temperature is most likely due to the thermal activation of minority carriers across the band gap E_g , which can be straightforwardly estimated from the peak thermopower α_{\max} and the temperature at which this maximum occurs T_{\max} via,

$$E_g = 2e\alpha_{\max}T_{\max}. \quad (1)$$

TABLE II. Room temperature values of the electron (n) and hole (p) concentrations, Seebeck coefficient (α), electrical resistivity (ρ), total thermal conductivity (κ), lattice (κ_L), and electronic (κ_e) thermal conductivity of $\text{Ba}_8\text{Au}_x\text{Si}_{46-x}$.

WDXS Au content	n (p) (10^{21} cm^{-3})	α ($\mu\text{V K}^{-1}$)	ρ ($\mu\Omega \text{ m}$)	κ ($\text{W m}^{-1} \text{ K}^{-1}$)	κ_e ($\text{W m}^{-1} \text{ K}^{-1}$)	κ_L ($\text{W m}^{-1} \text{ K}^{-1}$)
4.10	6.5	-12.0	5.2	3.5	1.50	2.0
4.85	4.1	-36.0	34.1	2.7	0.20	2.50
5.14	0.8	-104.0	33.2	1.7	0.15	1.55
5.43	0.8	143.2	58.6	1.5	0.10	1.40
5.59	1.5	108.2	23.6	1.6	0.30	1.30
6.10	7.2	47.0	6.6	2.2	1.15	1.05

This equation yields E_g values of 125 ± 5 meV, 112 ± 5 meV, and 150 ± 5 meV for the $x=5.14$, 5.43 , and 5.59 samples, respectively. These values are consistent with our band-structure calculations and those reported by Tse *et al.*¹⁷ Even though variations in E_g may indicate that a rigid-band model may not fully reflect the changes in the electronic band structure arising from Au substitution, assuming this approach provides a satisfying theoretical background to explain the temperature and composition dependence of the electrical transport properties in this system for both the n -type and p -type specimens. This is supported by a fairly constant effective mass of the charge carriers estimated at 300 K within a single parabolic band model.²¹ The latter conclusion still holds true at high temperature as illustrated in Figures 4(a) and 4(b), where the α values measured at 500 K are displayed as a function of the carrier concentration. As a first approximation, we

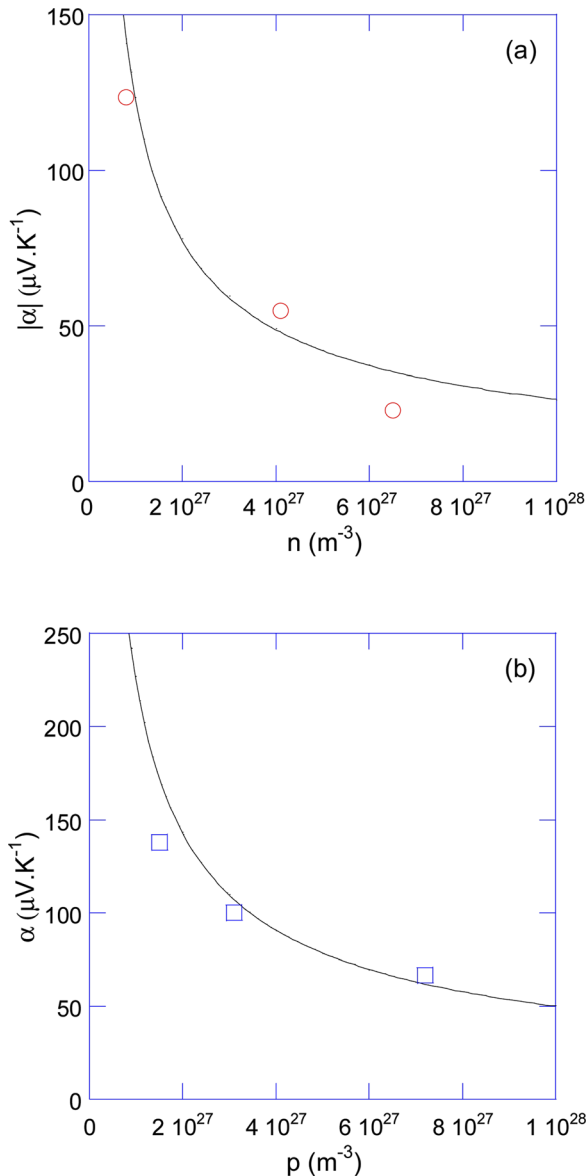


FIG. 4. (Color online) Carrier concentration dependence of the thermopower measured at 500 K of the (a) $x=4.10$, 4.85 , 5.14 samples and (b) of the 5.59 , 5.75 , and 6.10 samples compared to a single-parabolic band model with effective masses of 3.7 and $6.8m_0$, respectively.

considered the carrier concentration inferred from the Hall coefficient measured at 300 K (Table II) to be temperature-independent, except for the $x=5.43$ sample which clearly shows a semiconducting behaviour (see below). The data of this latter sample were therefore not included in the present analysis. Further, we employ this model at 500 K to ensure that extrinsic carriers still dominate the electronic transport. This approach would break down at higher temperatures since the contribution of the minority carriers is not included in the definition of the following equations, specifically in the $x=5.14$ and $x=5.59$ samples. Note that in order to extend this analysis to the p -type compounds, we measured $\alpha(T)$ of an additional sample with $x=5.75$. The so-called Pisarenko-Ioffe curves giving the variations in α with the carrier concentration, shown as solid lines in Figures 4(a) and 4(b), were generated by using the general solutions of the Boltzmann transport equation within the relaxation time approximation, for which the thermopower and the carrier concentration are linked via the reduced chemical potential η by²⁸

$$\alpha = -\frac{k_B}{e} \left(\frac{(2+\lambda)F_{1+\lambda}(\eta)}{(1+\lambda)F_\lambda(\eta)} - \eta \right), \quad (2)$$

$$p(n) = \frac{4}{\sqrt{\pi}} \left(\frac{2\pi m^* k_B T}{h^2} \right)^{\frac{3}{2}} F_{\frac{1}{2}}(\eta), \quad (3)$$

where k_B the Boltzmann constant, e is the elementary charge, h is the Planck constant, m^* is the effective mass of the charge carriers, λ is a scattering constant related to the energy dependence of the electronic scattering mechanism, and F_i is the Fermi integral of order i defined as $F_i(\eta) = \int_0^\infty \xi^i f_0(\xi, \eta) d\xi$, where f_0 is the Fermi distribution function and ξ is the reduced energy of electrons. Here, we assume that acoustic-phonon scattering is the dominant scattering mechanism of the charge carriers in the temperature range investigated for which $\lambda = 0$ as suggested by

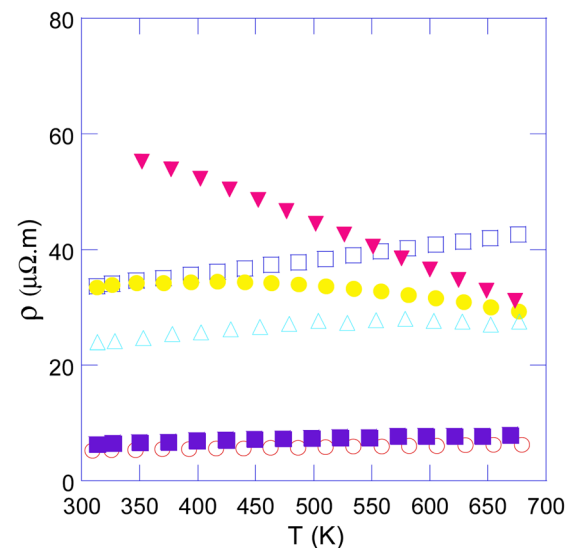


FIG. 5. (Color online) Temperature dependence of the electrical resistivity, ρ , of the $x=4.10$ (○), 4.85 (□), 5.14 (●), 5.43 (▼), 5.59 (Δ), and 6.10 (■) samples.

Hall data measured near room temperature.²¹ The curves were then calculated utilizing m^* values of $3.7m_0$ and $6.8m_0$ (m_0 is the electron mass) for the n -type and p -type samples, respectively, along with the carrier concentrations derived from Hall effect measurements. All the experimental data fall on or near this curve suggesting that the effective mass does not significantly vary within this carrier concentration range. This lends further support to a single-band model describing the conduction and valence band edges even at high temperatures. In addition, the larger m^* value in the p -type samples explains the higher values of $|\alpha|$ with respect to n -type samples with similar carrier concentration.²¹

The variations observed in the $\rho(T)$ (Figure 5) are consistent with the trends revealed by both the transport properties at low temperatures and the high-temperature thermopower data.²¹ The variations in the ρ values are also in agreement with this description and, as the $\alpha(T)$ data do, mainly reflect the changes in the carrier concentration with the Au content (Table II). A band gap of 145 ± 5 meV can be inferred from an Arrhenius plot of the high temperature region of the $\rho(T)$ curve for $x=5.43$, in reasonable agreement with the thermopower data.

B. Thermal properties

The temperature dependence of the specific heat, C_p , between 2 and 500 K for the $x=4.85$ and 5.59 samples is shown in Figures 6(a) and 6(b). Above room temperature, the C_p values increase with increasing temperature reflecting the anharmonic contribution of the lattice. In the present case, the Dulong-Petit law, usually used to estimate the C_p value at high temperature, overestimates the experimental value below ~ 500 K. This discrepancy is, however, not confined to this phase and was already found in several other Ge-based and Si-based type-I clathrates.¹³

The temperature dependence of the total thermal conductivity is shown in Figure 7. Upon warming, the thermal conductivity of the $x=5.14$, 5.43 , and 5.59 samples first decreases slightly before increasing at higher temperature. The coincidence of the maxima in the thermopower and the minima in the thermal conductivity consistently shows that the observed increase originates from the thermal activation of the minority carriers across the band gap, the simultaneous presence of holes and electrons resulting in an additional bipolar contribution κ_b . This contribution is most significant for samples exhibiting the lowest carrier concentration, i.e., for $x=5.14$ and 5.43 .

The detailed analysis of the Hall and thermopower data has shown that a model assuming a single parabolic-band with dominant acoustic phonon scattering provides a satisfying theoretical platform to describe the electrical properties of these samples. This model can be extended to the thermal transport to accurately assess the temperature dependence of the lattice thermal conductivity, κ_L , by subtracting the electronic contribution, κ_e , calculated via the Wiedemann-Franz law, $\kappa_e = LT/\rho$. Within the above-mentioned assumptions, the Lorenz number, L , obtained via solutions of the Boltzmann transport equation, is expressed as²⁸

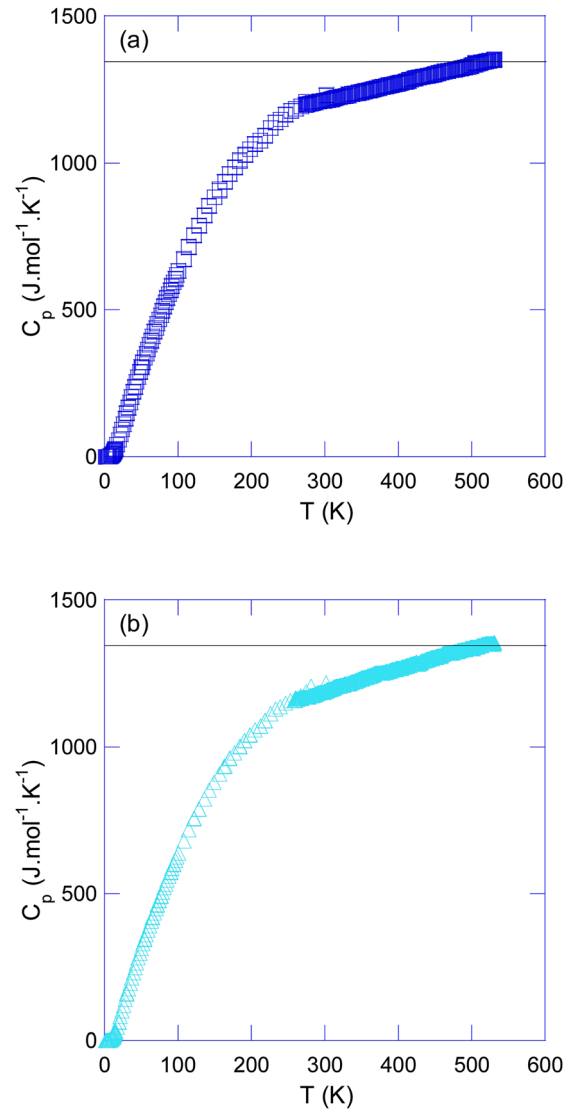


FIG. 6. (Color online) Temperature dependence of the specific heat, C_p , of the $x=4.10$ (a) and 6.10 (b) samples. The black solid line stands for the value expected from the Dulong-Petit law.

$$L = \frac{k_B^2 (1 + \lambda)(3 + \lambda)F_\lambda(\eta)F_{2+\lambda}(\eta) - (2 + \lambda)^2 F_{1+\lambda}(\eta)^2}{e^2 (1 + \lambda)^2 F_\lambda(\eta)^2}. \quad (4)$$

Using the η values derived from the thermopower data at high temperatures by Eq. (2), the temperature dependence of L can then be calculated and is depicted in Figure 8. As can be observed, the L values decrease with increasing temperature and are significantly smaller than that of a degenerate electron gas in a pure metal ($L = L_0 = 2.44 \times 10^{-8} \text{ V}^2 \text{ K}^{-2}$). At high temperatures, the values of the $x=5.14$ and 5.59 samples are only $\sim 20\%$ off the value for non-degenerate electron gas solely scattered by acoustic phonons ($L \approx 1.5 \times 10^{-8} \text{ V}^2 \text{ K}^{-2}$). The metallic behaviour of the $x=4.10$ sample indicates that assuming the metallic limit of L at high temperature is reasonable in the present case. For the $x=5.43$ sample, our description breaks down, the presence of both types of carriers above 300 K, which leads to an increase in κ , being not included in the definition of L .

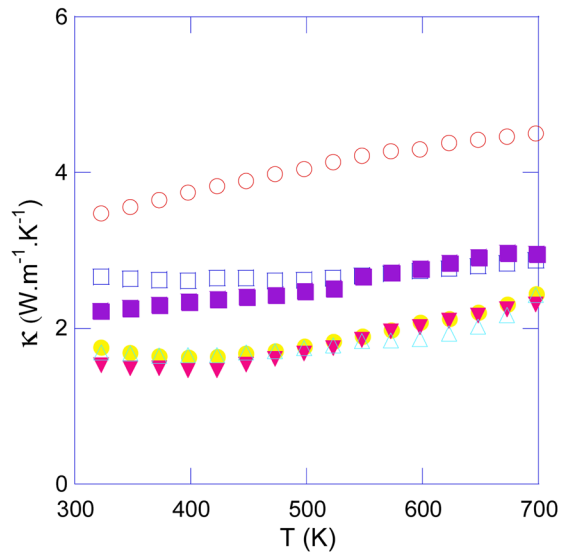


FIG. 7. (Color online) Temperature dependence of the total thermal conductivity, κ , of the $x=4.10$ (\circ), 4.85 (\square), 5.14 (\bullet), 5.43 (\blacktriangledown), 5.59 (\triangle), and 6.10 (\blacksquare) samples.

The temperature dependences of κ_e and κ_L in the whole temperature range investigated are shown in Figures 9(a) and 9(b), respectively. For $x \leq 5.14$, the curves are similar indicating a minimal influence of the Au content on the lattice contribution. Interestingly, $\kappa_L(T)$ significantly drops when crossing the n -type- p -type transition, the lowest values being achieved for $x=6.10$ (see Table II). As shown by the low-temperature data, the lattice thermal conductivity gradually shifts from a crystalline behaviour in the n -type samples to a glass-like one in the p -type samples.²¹ Several mechanisms have been discussed in the literature to explain such a difference in the thermal transport between n -type and p -type type-I clathrates such as tunnelling states, resonant scattering or a strong phonon-charge carrier coupling.^{6–9,29–34} Our low-temperature specific heat data along with x-ray diffraction

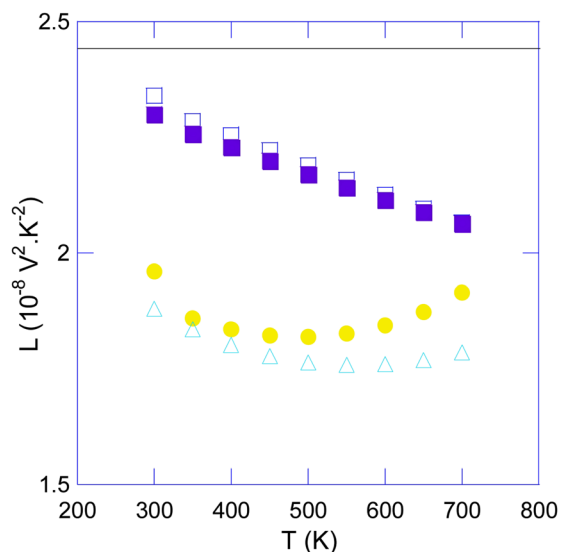


FIG. 8. (Color online) Lorenz number, L , as a function of the temperature for the $x=4.85$ (\square), 5.14 (\bullet), 5.59 (\triangle), and 6.10 (\blacksquare) samples. The values are significantly lower than the metallic limit represented by the solid black line and approach the value for non-degenerate electron gas scattered by acoustic phonons ($1.5 \times 10^{-8} \text{ V}^2 \text{ K}^{-2}$).

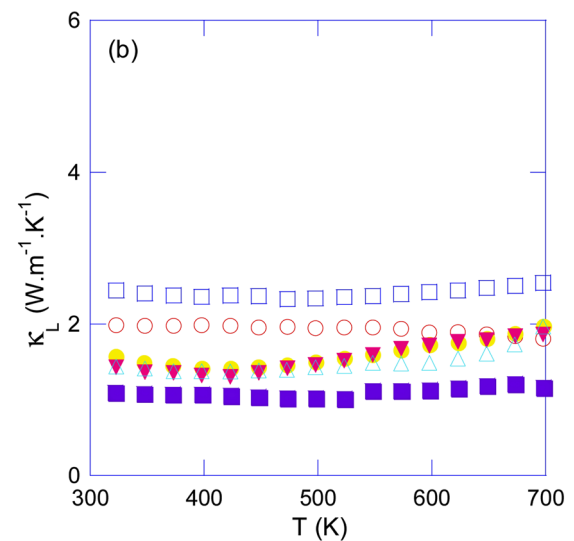
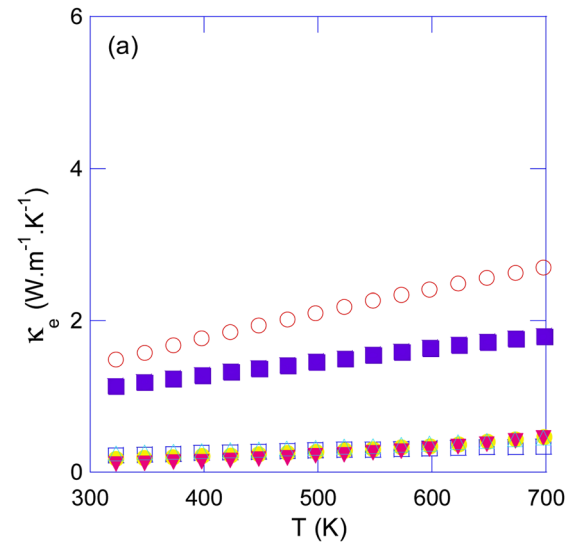


FIG. 9. (Color online) Temperature dependence of the electronic (a) and lattice thermal conductivity (b) of the $x=4.10$ (\circ), 4.85 (\square), 5.14 (\bullet), 5.43 (\blacktriangledown), 5.59 (\triangle), and 6.10 (\blacksquare) samples.

analyses have shown that tunnelling states are of minor importance in the present case.^{21,23} Though the presence of vacancies at high Au contents cannot be ruled out in the present case, the fact that Au is distributed on both the $6c$ and $24k$ sites might give rise to enhanced disorder and strain effects, thereby driving the disappearance of the low-temperature crystalline peak. This hypothesis seems to be supported by lower κ_L values measured in n -type $\text{Ba}_8\text{Ga}_{16}\text{Ge}_{30}$ ($0.14 \text{ W m}^{-1} \text{ K}^{-1}$ at 1000 K) for which the disorder induced by the presence of Ga on the three crystallographic Ge sites may play an important role.¹³ Additionally, the higher m^* values exhibited by the p -type samples may reflect a higher phonon-hole coupling which may as well contribute to the lower κ_L values observed.

From the electrical resistivity, thermopower and thermal conductivity data, the temperature dependence of ZT can be inferred and is depicted in Figure 10. A maximum ZT value of ~ 0.2 is achieved at around 600 K for $x=5.59$. It is, however, not surprising that this maximum value is obtained in

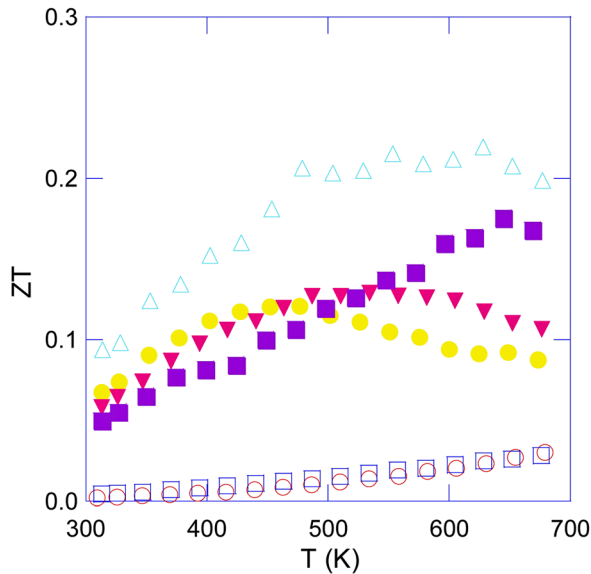


FIG. 10. (Color online) Temperature dependence of the dimensionless thermoelectric figure of merit ZT of the $x=4.10$ (\circ), 4.85 (\square), 5.14 (\bullet), 5.43 (\blacktriangledown), 5.59 (\triangle), and 6.10 (\blacksquare) samples.

one of the p -type samples since these exhibit higher thermopower values due to a higher effective mass and a lower thermal conductivity compared to the n -type samples. This maximum value is similar to those obtained in the $\text{Ba}_8\text{Al}_x\text{Si}_{46-x}$ and $\text{Ba}_{8-y}\text{Sr}_y\text{Al}_{14}\text{Si}_{32}$ systems for $x \sim 15$ and $y \sim 1$ ($ZT \sim 0.25$ at 1000 K and 0.3 at 1200 K, respectively) but remains lower than the one obtained in the Ga-substituted analogues (0.75 and 0.87 at 1000 and 850 K, respectively).^{11,18,20}

IV. CONCLUSION

Our investigations of the high-temperature thermoelectric properties of the clathrate $\text{Ba}_8\text{Au}_x\text{Si}_{46-x}$ revealed that the thermoelectric performance of this phase is lower than that of $\text{Ba}_8\text{Ga}_x\text{Si}_{46-x}$. While the thermal transport behaviour of the Au-based samples is similar to the Ga system with large effective mass and low thermal conductivity, the high electrical resistivity appears to be the limiting factor preventing to achieve a high ZT in the present series of samples (the maximum $ZT \sim 0.2$ is achieved at around 600 K for $x=5.59$). One of the main differences between these two systems lies in the possibility to switch the electrical transport from n -type to p -type behaviour by varying the Au content around $x=5.33$, in agreement with the Zintl-Klemm concept. All the electrical properties of both the n -type and p -type samples are well described by a single parabolic band model considering a single scattering mechanism of the charge carriers. To further optimize the thermoelectric properties of this material, it may be worthwhile to explore multiple substitutions to reduce the electrical resistivity while taking advantage of the low thermal conductivity values induced by substituting Si by Au. Another interesting way to this end may be by substituting alkali metals for Ba in the cages, enabling one to tune the carrier concentration and simultaneously enhance the disorder in the crystal structure.

ACKNOWLEDGMENTS

The authors thank Petra Scheppan, Renate Hempel-Weber, and members of the Kompetenzgruppe Struktur for providing experimental support. C.C. acknowledges the financial support of the CNRS-MPG program.

- ¹M. Christensen, S. Johnsen, and B. B. Iversen, *Dalton Trans.* **39**, 978 (2010).
- ²G. S. Nolas, G. A. Slack, and S. B. Schujman, *Semiconductors and Semimetals*, edited by T. M. Tritt (Academic Press, San Diego, 2001), Vol. 69, p. 255.
- ³K. A. Kovnir and A. V. Shevelkov, *Russ. Chem. Rev.* **73**, 923 (2004).
- ⁴J. L. Cohn, G. S. Nolas, V. Fessatidis, T. H. Metcalf, and G. A. Slack, *Phys. Rev. Lett.* **82**, 779 (1999).
- ⁵K. Suekuni, M. A. Avila, K. Umeo, and T. Takabatake, *Phys. Rev. B* **75**, 195210 (2007).
- ⁶M. A. Avila, K. Suekuni, K. Umeo, H. Fukuoka, S. Yamanaka, and T. Takabatake, *Phys. Rev. B* **74**, 125109 (2006).
- ⁷K. Suekuni, M. A. Avila, K. Umeo, H. Fukuoka, S. Yamanaka, T. Nakagawa, and T. Takabatake, *Phys. Rev. B* **77**, 235119 (2008).
- ⁸M. A. Avila, K. Suekuni, K. Umeo, H. Fukuoka, S. Yamanaka, and T. Takabatake, *Appl. Phys. Lett.* **92**, 041901 (2008).
- ⁹T. Mori, K. Iwamoto, S. Kushibiki, H. Honda, H. Matsumoto, N. Toyota, M. A. Avila, K. Suekuni, and T. Takabatake, *Phys. Rev. Lett.* **106**, 015501 (2011).
- ¹⁰H. J. Goldsmid, *Thermoelectric Refrigeration* (Temple Press Books Ltd., London, 1964).
- ¹¹D. Shu-Kang, T. Xin-Feng, and T. Run-Sheng, *Chin. Phys. B* **18**, 3084 (2009).
- ¹²V. L. Kuznetsov, L. A. Kuznetsova, A. E. Kaliazin, and D. M. Rowe, *J. Appl. Phys.* **87**, 7871 (2000).
- ¹³E. S. Toberer, M. Christensen, B. B. Iversen, and G. J. Snyder, *Phys. Rev. B* **77**, 075203 (2008).
- ¹⁴J. Martin, H. Wang, and G. S. Nolas, *Appl. Phys. Lett.* **92**, 222110 (2008).
- ¹⁵H. Schäfer, B. Eisenman, and W. Müller, *Angew. Chem., Int. Ed.* **12**, 694 (1973).
- ¹⁶*Chemistry, Structure, and Bonding of Zintl Phases and Ions*, edited by S. M. Kauzlarich (VCH publishers, Inc., New York, 1996).
- ¹⁷J. S. Tse, T. Itaka, T. Kume, H. Shimizu, K. Parlinski, H. Fukuoka, and S. Yamanaka, *Phys. Rev. B* **72**, 155441 (2005).
- ¹⁸N. Tsujii, J. H. Roudebush, A. Zevalkink, C. A. Cox-Uvarov, G. J. Snyder, and S. M. Kauzlarich, *J. Solid State Chem.* **184**, 1293 (2011).
- ¹⁹I. Zeiringer, E. Bauer, A. Grytsiv, P. Rogl, and H. Effenberger, *Jpn. J. Appl. Phys.* **50**, 05FA01 (2011).
- ²⁰J. H. Roudebush, E. S. Toberer, H. Hope, G. J. Snyder, and S. M. Kauzlarich, *J. Solid State Chem.* **184**, 1176 (2011).
- ²¹U. Aydemir, C. Candolfi, A. Ormeci, Y. Oztan, M. Baitinger, N. Oeschler, F. Steglich, and Yu. Grin, *Phys. Rev. B* **84**, 151137 (2011).
- ²²G. Cordier and P. Woll, *J. Less-Common Met.* **169**, 291 (1991).
- ²³N. Jaussaud, P. Gravereau, S. Pechev, B. Chevalier, M. Ménétrier, P. Dordor, R. Decourt, G. Goglio, C. Cros, and M. Pouchard, *C. R. Chim.* **8**, 39 (2005).
- ²⁴L. T. K. Nguyen, U. Aydemir, M. Baitinger, E. Bauer, H. Borrmann, U. Burkhardt, J. Custers, A. Haghhighrad, R. Höfler, K. D. Luther, et al., *Dalton Trans.* **39**, 1071 (2010).
- ²⁵H. Zhang, H. Borrmann, N. Oeschler, C. Candolfi, W. Schnelle, M. Schmidt, U. Burkhardt, M. Baitinger, J.-T. Zhao, and Yu. Grin, *Inorg. Chem.* **50**, 1250 (2011).
- ²⁶L. G. Akselrud, P. Y. Zavali, Yu. Grin, V. K. Pecharsky, B. Baumgartner, and E. Wölfel, *Mater. Sci. Forum* **133–136**, 335 (1993).
- ²⁷M. Falmbigl, G. Rogl, P. Rogl, M. Kriegisch, H. Müller, E. Bauer, M. Reinecker, and W. Schranz, *J. Appl. Phys.* **108**, 043529 (2010).
- ²⁸V. I. Fistul, *Heavily Doped Semiconductors* (Plenum, New York, 1969).
- ²⁹K. Umeo, M. A. Avila, T. Sakata, K. Suekuni, and T. Takabatake, *J. Phys. Soc. Jpn.* **74**, 2145 (2005).
- ³⁰J. Xu, J. Tung, K. Sato, Y. Tanabe, H. Miyasaka, M. Yamashita, S. Heguri, and K. Tanigaki, *Phys. Rev. B* **82**, 085206 (2010).
- ³¹B. C. Sales, B. C. Chakoumakos, R. Jin, J. R. Thompson, and D. Mandrus, *Phys. Rev. B* **63**, 245113 (2001).
- ³²A. Bienten, M. Christensen, J. D. Bryan, A. Sanchez, S. Paschen, F. Steglich, G. D. Stucky, and B. B. Iversen, *Phys. Rev. B* **69**, 045107 (2004).
- ³³M. Christensen, N. Lock, J. Overgaard, and B. B. Iversen, *J. Am. Chem. Soc.* **128**, 15657 (2006).
- ³⁴A. Bienten, S. Johnsen, and B. B. Iversen, *Phys. Rev. B* **73**, 094301 (2006).